Design of a Humanoid Hand
Using Segmented Shape Memory Alloy Actuators

by

Josiah Benjamin Rosmarin

SUBMITTED TO THE DEPARTMENT OF MECHANICAL ENGINEERING IN PARTIAL FULFILLMENT OF THE REQUIREMENTS FOR THE DEGREE OF

BACHELOR OF SCIENCE
AT THE
MASSACHUSETTS INSTITUTE OF TECHNOLOGY

JUNE 2006

Signature of Author: _____
Department of Mechanical Engineering
5/12/2006

Certified by: _____
H. Harry Asada
Professor of Mechanical Engineering
Thesis Supervisor

Accepted by: _____
John H. Lienhard V
Professor of Mechanical Engineering
Chairman, Undergraduate Thesis Committee

Design of a Humanoid Hand
Using Segmented Shape Memory Alloy Actuators

by

Josiah Benjamin Rosmarin

Submitted to the Department of Mechanical Engineering
on May 12, 2006 in partial fulfillment of the requirements
for the Degree of Bachelor of Science in Mechanical Engineering

ABSTRACT

Despite amazing progress in the past two decades, the field of robotics has yet to produce a robotic hand with the same dexterity as the human hand. There has yet to even be a functioning robotic hand of the same size and weight as the human hand. These deficiencies can be attributed to the size, weight and complexity of the actuators used in these robotic hands. Thermal shape memory alloys (SMA's) have characteristics such as high power density which indicate that they would be ideal actuators for such applications. However, certain characteristics of SMA exist which, if left unaddressed, make usage as an actuator impractical. The implementation of SMA for the actuation of a 20 degree of freedom robotic hand and forearm is investigated. A segmented actuation design for the SMA is implemented to address issues of practicality; other issues with regards to the controllability, response time and limited strain of the SMA are addressed. A 20 degree of freedom robotic hand with 16 controlled axes is designed along with a 32 axis actuator box. The designs are realized and the result is a functioning robotic hand of similar size and weight to the human hand. It is concluded that thermal shape memory alloys are a viable solution for the purposes of compact lightweight actuation of vast degree of freedom systems.

Thesis Supervisor: H. Harry Asada

Title: Professor of Mechanical Engineering

Table of Contents

1. Introduction

The field of robotics, to many, has become not only an area of scientific interest but an obsession. Many fields exist within the broader realm of robotics, but the field of biomimetics has earned a special degree of interest for many reasons, some practical and some philosophical. Within the field of biomimetics, the most popular physiology to mimic is, of course, the human physiology.

The underlying idea of biomimetics is that the engineering for the specific mechanisms in question has already been done, basically that the naturally occurring mechanisms already work. Obviously, the object of this field is not to identically recreate the mechanisms, so much as to use them as a basis for design. It is often the deviations from the natural model, rather than the similarities which draw the most scientific interest. This is because it is the deviations from the natural model which are responsible for different behavior. This can be a good or bad thing, depending on the requirements for the mechanism. Deciding which mechanism is 'better' is often not a clear task; often times it depends on the details of the test.

In any case, even with millions of dollars and thousands of hours of research put into the task of developing, the human hand outperforms any artificial hand produced in all but very highly specialized tests. The analysis of the host of robotic hands that have been developed can lead to very specific shortcomings in the area of robotics as a whole. A complete solution cannot be presented, however clear improvements can still be made.

1.1. Literature Survey

This section identifies several major contributions to the field of anthropomorphic robotic hands. This list presented below is not by any means an exhaustive list but rather a cross-section of the many robotic hands that have been developed in order to get a general idea of the state of

the field. It can be noted that the actual performance of the robotic hands is not addressed but rather the general mechanical structure. This is because it is not easy to quantify performance objectively. Many of these hands have videos demonstrating performance, but even the videos demonstrate the hands performing in very controlled environments. It is quite apparent that a significant amount of progress can still be made in the field. The hands which are considered are presented in chronological order.

One of the very first anthropomorphic hands, and probably the first noteworthy one, was the Okada Hand [1]. The Okada Hand was developed in the Electrotechnical Laboratory in Japan and presented to the public in 1979. It only had two fingers and a thumb and was significantly larger than the human hand; it had a total of 11 joints and 11 degrees of freedom. The hand was driven by DC motors which were remotely located and connected to the joints via sheathed tendons. The development of this hand set a new standard in the field.

The next major development was the Stanford/JPL Hand which was made public in 1983 [2]. It also had two fingers and a thumb, with 9 joints and 9 degrees of freedom. This hand was also driven by remotely located DC motors, actuating the joints with sheathed tendons. It was designed to manipulate objects only at the fingertips, which were each fitted with an array of tactile sensors. The hand was developed for the study of grasp stability.

Around the same time as the Stanford/JPL Hand, the Utah/MIT Hand was released [3]. The Utah/MIT hand was significantly more complex with three fingers and a thumb; it had 16 joints and 16 controlled degrees of freedom. This hand utilized pneumatic actuators which were located remotely and connected to the joints by tendons. The surfaces of the fingertips, the fingers and the palm were all designed to be usable for contact with objects for manipulation. This allowed for a control scheme more similar to that employed by the actual human hand.

In 1992, a hand by the name of UB Hand II was released by Bologna University [4]. This hand only had two fingers and a thumb, with 13 joints and 13 degrees of freedom. This hand was also actuated by DC motors with sheathed tendon power transmission. Of note with this hand was the highly anthropomorphic design of each of the individual fingers, the revolutionary joint design and the innovative tendon routing to avoid coupling the motion of the joints of the fingers.

The first DLR Hand was released in 1997 [5]. While this hand is significantly larger than the human hand, it has the interesting feature of directly driven joints. The actuators for the motion of the fingers are located inside the fingers themselves. This hand consists of three fingers and a thumb. Also of note, each of the fingers in this hand is underactuated, allowing for a mechanical grasp adaptation independent of complex control algorithms, mimicking the actual actuation structure of the human hand.

The Robonaut Hand was released by NASA in 1999, and is arguably a leader in the field. This five fingered hand has 20 joints and 12 actuated degrees of freedom, as well as a fully controlled 2 d.o.f. wrist. The actuation is done by brushless DC motors which power lead screws. The power is transmitted via flexible shafts. The index and middle fingers of this hand each have four fully controlled degrees of freedom. The other two fingers, while having three joints, each only have one actuator. This hand has a very large workspace and is covered in surfaces which can be used in grasping. This hand is quite effective and there are many videos demonstrating the achieved level of dexterity.

One of the leading commercially available robotic hands is manufactured by Shadow Robot Company Ltd. This hand is characterized by having as many or even more controlled degrees of freedom as the human hand. It has four fingers, each with four degrees of freedom,

and a thumb which has five degrees of freedom, and the palm can even cup, as in the human hand. This hand is actuated by a pneumatic system which transmits power to the joints via a system of tendons.

1.2. General Shortcomings of Robotic Hands

Not a single hand presented demonstrated the level of dexterity found in the human hand; all of the hands presented were either significantly larger than the human hand, had bulky actuator systems, or reduced controlled degrees of freedom compared to the human hand. There were some impressive demonstrations, including a video of Robonaut hand passing a screwdriver from a grasp between the thumb and middle finger to a grasp between the index and middle fingers. However, if that demonstration were to be done by a human, it would be less than impressive. This is one indication that the field has significant work to be done.

While it is very clear that there is no robotic hand that even approaches the efficacy of the human hand in applications in which the human hand is normally used, it is no simple task to quantify these shortcomings. While there is no hand as *versatile* as the human hand, there are plenty of hands that are *stronger, quicker,* and with a larger *workspace.* However when these hands are subjected to simple tasks, such as opening a door by turning a doorknob, it becomes quite clear that the performance of the human hand is far superior. The measure of this ability to effectively manipulate objects in complex manners is commonly referred to as dexterity.

It has been identified that the major deficiency in the dexterity of robotic hands can be attributed to control schemes and sensor systems [6]. It is quite obvious that significant research in these fields has yet to be done, but these fields are not the sole source of the blame. Much work in the purely mechanical fields has yet to be accomplished. This paper will focus on the mechanical issues, specifically in making advances in the field from a practical perspective.

One common attribute in all of the functioning hands was the fact that the weight and volume of the actuators were significantly greater than the weight and volume of the muscles which actuate the human hand, ranging from around three times the volume to orders of magnitude larger. Practically speaking, from the perspective of humanoid robotics and especially prosthetics, this is simply unacceptable. Since the commonly used actuators generally take up such a large volume, it would make sense that it may be advantageous to depart from standard actuators in order to achieve a compact design.

It will be demonstrated in this paper that certain thermal shape memory alloys (SMA) can be used in such a way as to reduce the size of the actuators and robotic hand to the size of the actual human hand and forearm, while still maintaining the general mechanical performance of the human hand, more specifically what is referred to by [6] as 'mechanical potential dexterity', and without impeding the ability to implement a sufficient control scheme.

2. Approach

A superficial analysis of the properties of the wide range of available actuators reveals that thermal shape memory alloys are by far the most compact class of actuators. However, many issues arise with implementation which have significant effects on not only the volume, but also on controllability and which introduce significant complications. For this reason, they still are not widely accepted as a clear solution. In the next few sections I will briefly justify the selection of NiTi as an actuator, identify some key issues with NiTi as an actuator, and then address these issues.

2.1. Actuator Selection

Since human muscle has already proven itself as a very capable actuator in an already proven mechanical design, namely the human hand, it was chosen as the baseline for the

evaluation of the performance characteristics of the actuators which were considered. The evaluation of the actuators was done from a practical perspective, evaluating not only their raw characteristics but also how they would perform in the actual application of this concept. For instance, a DC motor may have some maximum power output and have some specified volume, leading to a simple calculation for peak power density. However, it may be necessary to include a gear box to achieve sufficient torque outputs, and it is necessary to include a pulley to convert the rotational motion into linear motion. The necessary additional mechanical components may end up taking up more room than the DC motors themselves, and thus should be included in the calculation of power density.

The baseline actuator would logically be muscle tissue. It would seem that since muscle is a very complex nonisotropic organic tissue, the peak stress that any particular muscle would be capable of producing would widely vary and depend on a variety of parameters. It turns out that the peak stress generated by muscle is quite constant throughout not only the entire human population, but also the entire phylum of vertebrates: 350 kPa [7]. Muscle tissue, however, is only capable of sustaining such large stresses for brief periods of time due to fatigue. Human muscle can only sustain around 30% of the maximum peak stress, or 100 kPa [8]. Human muscle is capable of undergoing a maximum strain of around 40%, has a maximum work density of approximately 40 kJ/m^3, and has a maximum power density of 284 W/kg [9]. It can be noted that since these properties are obtained from within the context of actuating the movements of the human body, they are applicable in their current state and thus do not need any further calculations.

In contrast to human muscle, the shape memory alloy known as "Nitinol" (or NiTi) is often called an artificial muscle, due to its superficially similar behavior to muscle tissue.

Nitinol was developed in the 1960's in the Naval Ordnance Laboratory. It is known as a shape memory alloy because it can exist in two different solid phases, depending on its energy levels, which are characterized by different crystallographic configurations. These different molecular configurations can lead to significantly different macroscopic geometries. Thus, an object made from such a material can return to a shape after being drastically changed simply by undergoing a phase transition.

This phase transition can be effected in different ways, but in the context of robotics, the relevant ways are stress and heat. The material can be formed and treated in such a way as to allow up to an 8% strain in between phases [9]. The stress in the material associated with this phase transition is in excess of 200 MPa, the maximum power density is approximately 50 kW/kg [8], and the maximum associated work density is around 10 MJ/m^3. It should be noted that the above properties of NiTi appear to outperform human muscle in excess of two orders of magnitude. However, as will be described in more detail later, a significant amount of additional space is needed in order to allow the material to cool.

In comparison, a DC motor has significantly poorer characteristics. Since DC motors are mechanical devices rather than solid materials, it is much more difficult to ascribe to it exact numbers in relation to performance characteristics. For reference, a specific DC motor is chosen to compare to the other actuators. This motor, the LC22G-103, is produced by copal electronics; the data can be found at http://www.copal-electronics.com. This motor has a maximum power output of around 10W, and weighs around 60g, thus giving a peak power density of around 170 W/kg. For comparison, this is around 1/300 the power density of SMA.

There exist a wide range of other materials which can be used as actuators. The following table was compiled from data from [7], [8] and [9].

Table 1: Relevant Characteristics of Actuator Materials

	Muscle	Ferromagnetic SMA	Thermal SMA	Conducting Polymers	Liquid Crystal Elastomers
Power Density (W/kg)	284	n/a	50,000	150	1
Work Density (kJ/m^3)	40	100	10,000	100	3-56
Maximum Stress (kPa)	350	9,000	200,000	34,000	10-120
Maximum Strain (%)	40	10	8	12	19-45

The above table highlights some of the key characteristics of thermal shape memory alloys that made them appear to be the clear choice for selection as the actuator for a robotic hand. However, there are many issues with both the control and implementation of shape memory alloys that need to be identified and addressed.

2.2. Issues with SMA for Robotic Hands

The most salient complication introduced by SMA is its limited controllability. Thermal SMA's, as indicated by the name, are actuated by heat, but the relation between the strain and temperature is anything but linear. This is due to the nature of the contraction of thermal shape memory alloys.

Generally, solid materials undergo a strain due to a change in temperature, expanding linearly to a rise in temperature. SMA actuators actually shrink when exposed to certain increases in temperature; this is because SMA's can exist in two different phases, known as Austenite and Martensite. The crystallographic configuration of Austenite is face centered cubic, while that of Martensite is body centered tetragonal. The configuration of Austenite is a higher energy configuration and thus can be attained by increasing the temperature of the compound. The specific energy of this transformation is a complex function involving the chemical composition (ratio of nickel to titanium), the stress the material is experiencing and possibly many other factors.

In order to control the length of the wire with any precision, it then becomes necessary to

not only know the temperature of the wire, but also to know other conditions of the wire, such as the tension in the wire. However, even if all such information were present, there is another factor which complicates controls: There is a hysteresis in the strain. The transition temperature to go from Austenite to Martensite is significantly lower than the transition temperature from Martensite to Austenite. Thus, any overshoot in the controls would require an extremely large change in temperature to resolve. Coupling this with the complexity of the knowledge of the state of the material necessary for controls, it becomes clear that precise control of the exact amount of strain in the SMA is a nontrivial task.

The limited controllability is not the only complication that arises with the use of thermal shape memory alloys: shape memory alloys have a very limited reaction time. In order to undergo a complete phase change the material has to experience a 40 K change in temperature (see Appendix I). While heating the material can be accomplished quite rapidly, the cooling time is generally the limiting factor. When dealing with natural convection at room temperature, the cooling time could be on the order of a couple of seconds!

Another issue with shape memory alloys is the limited strain. Even though shape memory alloys have very high power density, the majority of it is due to the extremely high stress in the material. While the maximum strain that can be achieved by the material is 8%, it is not practical to use it for strains larger than 5% [8]. This is about 1/8 of the strain that human muscle is capable of producing. Thus, in order to achieve the same torques over the same range of motion, shape memory alloys will produce internal forces eight times as great as those produced by human muscle.

The final major issue with shape memory alloys is the energy efficiency. The majority of the energy put into SMA goes to cause it to undergo the phase transition. Very little of it is

turned into usable mechanical energy. Shape memory alloys are less than 5% efficient.

2.3. Approach

Many serious issues with Thermal SMA's have been raised. These issues, when left unaddressed, make SMA's ineffective, or at the very least impractical. However each of these issues can be addressed in a very simple and practical ways as will be explained below.

2.3.1 Controllability

It was stated earlier that SMA has limited controllability. It would be more correct, however, to say that it has a limited controllability in the conventional sense. An intuitive way to control the contraction of the material would be to vary the temperature of the entire wire in order to get a continuous variation of length in the wire. This, however, as indicated earlier, involves complex modeling and almost a full knowledge of the state of the material. In order to effectively use SMA, it seems almost necessary to approach the controls in a different way.

While it is difficult to precisely control the exact percentage of strain of SMA, it is not difficult to ensure that all of the material in the actuator undergoes the phase transition. Thus, it is easy to cause the actuator to alternate between maximum and minimum length, as long as it is not necessary to achieve intermediate lengths. This limitation when implemented in applications which require large amounts of precision, such as a robotic hand, is simply unacceptable.

However, it can be noted that human muscle behaves in the exact same way. When actuated, a sarcomere can only completely contract, it is unable to undergo a partial contraction [10]. This is sometimes called the "all or none" principle. In this sense, human muscle behaves quite analogously to the shape memory alloys. However, the resolution of the movement of human extremities is very high. This is because human muscles consist of a multitude of individual fibers, a number sufficient to approximate an almost continuous motion.

A joule-heated SMA wire with an electrode on either end (the standard configuration) is the equivalent to a single muscle fiber. Since it is general practice to have a single SMA wire actuate a single axis; this situation is analogous to a single-fibered muscle. However, it would prove to be much more beneficial to develop a strategy in which the SMA wire would be equivalent to several individual fibers.

Enter the idea of segmentation. By breaking the wire up into several discrete segments, each individually activated, it is possible to recreate a similar behavior within the SMA wire. In order to implement this solution, however, two issues must be addressed. The first is figuring out exactly what resolution is needed. The second is to figure out if heating in segments truly leads to separation of actuation. Specifically, since that material is activated by heat, the question is whether or not the thermal resistance high enough to sufficiently impede the spread of heat beyond the desired regions. Since this question is more fundamental, it will be the first to be addressed.

Figure 1: An SMA wire approximated as an infinitely long fin*

2.3.1 Justification of Segmentation

The ratio of the length to the radius of a typical SMA wire is approximately 2000:1, and therefore can be modeled as an infinitely long fin. It can be assumed that the heated side of the wire is held at a constant temperature. The point $x = 0$ is the boundary between the section of wire that is supposed to be heated and the section of wire which is not. The temperature distribution in an infinitely long fin is described by the equation,

* It should be noted that many of the following calculations are based on thermodynamic correlations, and as such require actual values rather than pure variables in order to determine which correlation is applicable. As such, the values used for the calculations in this section are the values of the actual parameters of the final design.

$$\frac{T_{(x)}-T_{\infty}}{T_H-T_{\infty}}=e^{-\left(\sqrt{\frac{h_c p}{kA_c}}\right)x} \tag{1}$$

where $T(x)$ is the temperature, x is the distance from the boundary, T_∞ is the ambient temperature, T_H is the temperature of the heated end, h_c is the coefficient of convection, p is the perimeter, k is the thermal conductivity of the fin material, and A_c is the cross-sectional area. Since we are dealing with a cylinder we can further simplify this equation; it would also prove useful to rearrange this equation to yield the distance from the boundary for any given temperature. Since we know the transition temperature and the temperature to which it will be heated, we can find the length of wire which is activated that is not supposed to be. That equation is as follows:

$$x=\ln\left(\frac{T_H-T_{\infty}}{T(x)-T_{\infty}}\right)\sqrt{\frac{r_0 k}{2h_c}} \tag{2}$$

where r_0 is the radius of the wire.

The majority of the terms in (2) are quite readily available. The transition temperature of the SMA used is around 90° C. Thus, the temperature to which the wire will be heated (T_H) is likely to be 100° C. The minimum temperature at which any significant percentage of the SMA will be undergoing a phase change ($T(x)$) would be around 75°C. Room temperature (T_∞) is approximately 22°C. The thermal conductivity (k) of SMA is around 20.92 W/m·K, and the radius of the SMA (r_0) is 191 μm. However, the coefficient of thermal convection (h) must be calculated.

The coefficient of thermal convection can vary quite widely depending on a range of parameters. Since it is clearly in the best interests of the performance to use forced convection for cooling (which will be discussed later) the coefficient of thermal convection will be calculated for only that set of conditions.

When calculating convection, the first step is always to characterize the flow; if it is

laminar it will respond quite differently than if it is turbulent. This is accomplished by calculating the Reynolds number, which is the ratio of the viscous forces to the inertial forces and is characterized by the below equation,

$$\mathrm{Re} = \frac{\rho v D}{\mu}. \tag{3}$$

Where ρ is the density of the fluid, v is the velocity of the fluid, D is the diameter of the relevant object (in this case the SMA wires), and μ is the viscosity of the fluid. At room temperature, air has a density of 1.169 kg/m^3, and a viscosity of $18.491\text{x}10^{-6}$ kg/m·s. The diameter of the SMA wires is $381\text{x}10^{-6}$ m. The velocity of the air produced by the fans is 2.307 m/s. By (3) the Reynolds number is therefore 55.574.

The next step in determining the convection coefficient is determining the Prandtl number, which is the ratio of the thermal diffusivity to the momentum diffusivity. This is a much simpler task since all of the parameters in determining the Prandtl number are material specific:

$$\mathrm{Pr} = \frac{\mu c_p}{k} \tag{4}$$

where c_p is the specific heat, k is the thermal conductivity, and μ is the viscosity. For air, since μ $=18.491\text{x}10^{-6}$ kg/m·s, c_p = 1006.6 J/kg·K, and k = 0.026 W/m·K, equation (4) yields that Pr = 0.7134.

The next step in calculating the coefficient of thermal convection is to find the Nusselt number, which characterizes the enhancement of heat transfer versus the thermal conductivity of a fluid. It is described by the following equation:

$$\mathrm{Nu} = \frac{h_c D}{k} \tag{5}$$

where h_c is the coefficient of thermal convection, D is the characteristic length, and k is the thermal conductivity of the fluid. The work done by Churchill and Bernstein [12] indicates that for Reynolds numbers under 10000 and Prandtl numbers above 0.5, the following correlation approximates Nu:

$$\mathrm{Nu} = 0.3 + \frac{0.62\,\mathrm{Re}^{\frac{1}{2}}\,\mathrm{Pr}^{\frac{1}{3}}}{\left(1+\left(\frac{0.4}{\mathrm{Pr}}\right)^{\frac{2}{3}}\right)^{\frac{1}{4}}} \tag{6}$$

Applying our values that we have obtained for the Prandtl and Reynolds number, we arrive at Nu = 3.927. Applying equation (5) we finally arrive at a value for the coefficient of convection, h_c = 269 W/m²K. Applying this information to equation (2), we arrive at the length of unintentionally activated SMA: 406 μm. This number will be important in determining the limit of attainable resolution.

With regards to the resolution needed to recreate the functionality of the human hand, the answer is quite task dependant. Analysis of the most common grasping motions and configurations of the human hand was done by [11] in order to determine the coupling of the actuation of the human fingers. This gives insight into exactly what resolution is needed.

2.3.2 Response Time

The response time of the material can be divided into two categories: contraction and relaxation. The contraction is caused by heating and the relaxation is caused by cooling. Therefore, the limitation of the reaction of the contraction of SMA is more or less how quickly energy can be dumped into it. The most common method of heating the material is by running electrical current through it, which is known as joule heating. The cooling of the material is generally the limiting factor, due to the constraints placed by the second law of thermodynamics.

Joule heating is generally chosen as the method of heating for several reasons. The

electrical resistance of thermal SMA's is relatively high for most metals; as such, the current needed to heat the wire is significantly less. Another reason to use joule heating is simplicity. Generally controls are done by electronics, and joule heating requires no extra equipment beyond the power circuitry. The energy needed to cause the material to transition from Martensite to Austenite is divided in two tasks. The first is to increase the temperature of the material to the transition temperature, and the second is to supply the energy needed to undergo the crystallographic transformation.

The energy needed to increase the temperature is characterized by

$$U = mc_p \Delta T \tag{7}$$

where U is the energy, m is the mass of the material, cp is the specific heat of the material and ΔT is the change in temperature of the material. The specific heat of SMA is 837 J/kg-K, and the difference of room temperature and the transition temperature is 68 K. From (7), the energy per unit mass needed to bring SMA from room temperature to its transition temperature is 57 kJ/kg. Similarly, the energy per unit mass needed to undergo the phase transition is 24 kJ/kg (see Appendix I). Thus, in order to bring Martensite at room temperature to Austenite, 81 kJ/kg is needed.

The power dissipated by an electric current in a material of constant cross-section and resistivity is characterized by

$$P = I^2 R, \tag{8}$$

where P is the power, I is the current, and R is the resistance of the material. This can be described by the equation

$$R = \frac{\rho_e l}{A_c}, \tag{9}$$

where ρ_e is the electrical resistivity, l is the length of the wire, and A_c is the cross-sectional area. The mass of the wire can be found by the equation

$$m = \rho_m V = \rho_m A_c l \tag{10}$$

where m is the mass, ρ_m is the density, and V is the volume of the wire. The change in thermal energy stored in the material is given by the expression is given by (7). Similarly, the heat dissipated by the material will be given by the equation

$$\dot{Q} = hA_s \Delta T \tag{11}$$

where A_s is the surface area and T is the difference between the material temperature and the ambient temperature, and h is the coefficient of convection. Combining (7), (8) and (11) yields a differential equation which will yield the heating time.

$$t = \frac{mc_p}{hA_s} \ln\left(\frac{T_0 - \left(T_\infty + \frac{I^2 R}{hA_s}\right)}{T_f - \left(T_\infty + \frac{I^2 R}{hA_s}\right)}\right) + \frac{U_t}{I^2 R - hA_s\left(T_f - T_\infty\right)} \tag{12}$$

The response time, therefore is limited only by the amount of current that can be delivered.

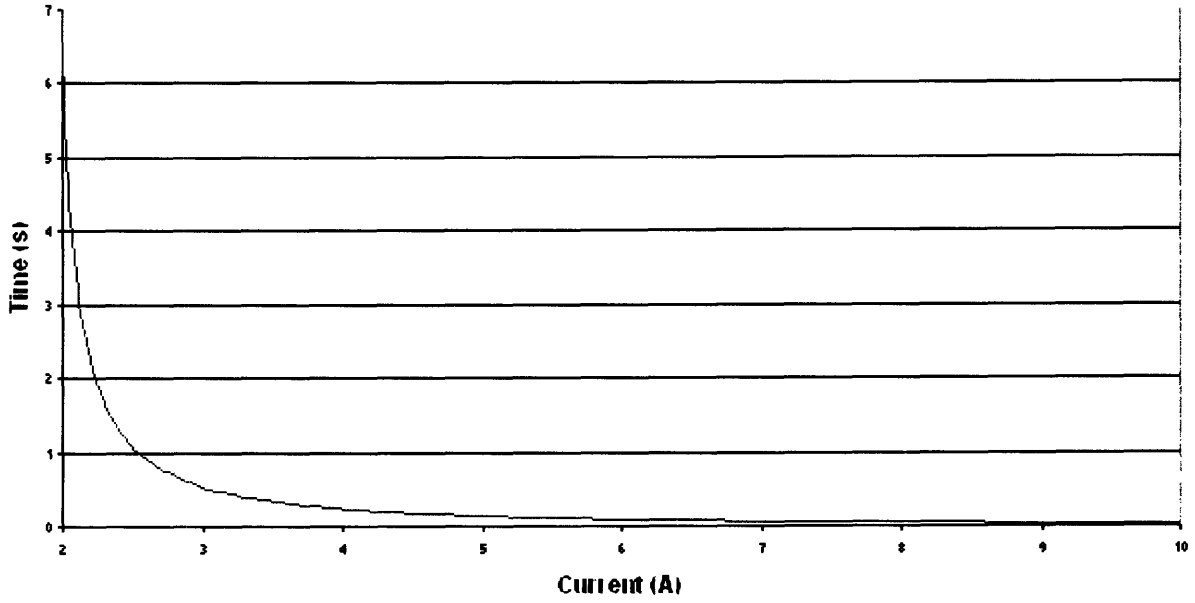

Figure 2: A plot of the response time of the system as a function of the input current.

With regards to relaxation, however, improving the cooling time is not as simple as increasing a current. In order to determine the cooling time, it is necessary to once again characterize the system. By far the simplest characterization of the cooling process would be the lumped thermal capacitance model. In order to be justified in making this approximation, the Biot number must first be calculated. The Biot number characterizes the ratio of the thermal resistance between an object and its surroundings to the thermal resistance within the object. The Biot number is described by the equation

$$\mathrm{Bi} = \frac{h_c l}{k} \tag{13}$$

where h_c is the coefficient of thermal convection, l is the characteristic length, and k is the conductivity of the material. Using the radius of the SMA wire as the characteristic length, (13) yields that Bi = 1.652×10^{-3}. This number indicates that the lumped thermal capacitance model is a good approximation.

The lumped thermal capacitance model yields that the temperature at any given time is described by the equation

$$T_{(t)} = T_0 e^{-\left(\frac{A_s h}{mc_p}\right)t} + T_\infty \left(1 - e^{-\left(\frac{A_s h}{mc_p}\right)t}\right) \tag{14}$$

where T_0 is the initial temperature, T_∞ is the ambient temperature, A_s is the surface area, h is the convection coefficient, m is the mass, and c_p is the specific heat. This can be rearranged to yield an expression for the time needed for a thermal capacitor to reach a specific temperature:

$$t = \frac{r_0 \rho_m c_p}{2h} \ln\left(\frac{T_0 - T_\infty}{T - T_\infty}\right) \tag{14a}$$

where T is the final temperature of the thermal capacitor, and t is the time it took to reach that

temperature. This time corresponds to the time needed to reach the transition temperature but does not include the time needed to undergo the transition. This value can be calculated by (11). Since the temperature of the material stays constant throughout the transition, the rate of heat dissipation also stays constant. The time of this process is therefore represented by the equation

$$t = \frac{U}{\dot{Q}} = \frac{U}{hA_s\Delta T} \tag{16}$$

where U is the total energy of the transition. The combination of (14a) and (16) yields the total cooling time:

$$t = \frac{r_0\rho_m c_p}{2h}\ln\left(\frac{T_0 - T_\infty}{T - T_\infty}\right) + \frac{U}{hA_s\Delta T} \tag{17}$$

Assuming an initial temperature of 100° C, well above the transition temperature, a final temperature of 65° C, and an ambient temperature of 22° C, and including the known density and specific heat of SMA, as well as the radius of the actuator, the only parameter left to be determined is the coefficient of convection. Assuming (overestimating) h = 25 W/m²K a cooling time can be approximated at 12 seconds. The cooling time, however, can be greatly improved in several different ways. For instance, by introducing forced convection from a miniature computer case fan, the cooling time is reduced to 1.14 s as calculated from (14a).

The other possible solution would be to lower the ambient temperature. However, the dependence of the response time due to changes in temperature is logarithmic, and the nature of temperature makes the minimum achievable temperature limited as well. Even if the ambient temperature were brought to 0 K, the response time would only be improved by a factor of 9!

Since the improvements attained by an ordinary case fan are more significant than the improvements made by a practically impossible temperature drop, it becomes apparent that this simple solution has serious merit.

2.3.3 Addressing other issues

While the strain undergone by shape memory alloys (5%) is significant compared to other metals, practically speaking, it is very small. This, however, is not a fatal limitation. In fact, this limited strain can be used advantageously. By taking advantage of simple mechanical advantages, the same motions can be realized, but since the strain is smaller, the corresponding radii of mechanical structures which utilize full stroke length will be smaller. This leads to a more compact design. While this does increase internal forces, the increased amount of material is not significant compared to the decrease in size of the apparatus. This will become more apparent when implemented.

One significant issue with shape memory alloys is the power efficiency. Shape memory alloys have an efficiency that ranges from 2-5%. However, the work that will be done by shape memory alloys is mostly the reconfiguration of fingers and the manipulation of objects. By avoiding tasks in which a large amount of work is necessary, the small efficiency becomes significantly less of a problem.

Human muscle, while efficient when dealing with motion, turns out to be quite inefficient at sustaining forces. Shape memory alloys are exactly the opposite. It does not take large amounts of energy to maintain a position, but changes in configuration are characterized by a low inefficiency. Thus, by implementing control schemes which take this into consideration, much less energy will be wasted. For instance, if a heavy object needs to be lifted, if the robot hand were to first tightly grasp an object (using SMA) before attempting to move it (with some other actuator) the SMA would retain its position without wasting energy, and therefore maximize efficiency. By contrast, if the control scheme were to include grasp alteration after the object was already lifted, large amounts of energy would be wasted and the low efficiency of

SMA would become quite apparent.

However, taking all things into consideration, the normal tasks performed by the human hand are low-energy. When a person lifts a heavy object, they do not rely on a pinch grasp of their fingers; they instead anchor the object against their palm or rest it at the base of the thumb. In the same way, a robotic hand will only be used in low-energy applications. As such the efficiency is not as essential as other parameters.

3. Design Considerations

As shown above, there are several abstract issues with even the concept of using SMA as an actuator. However, there are even more practical issues when it is implemented. The below section delineates the approach used to design the robotic hand, breaking the process into three sections: actuator parameter selection, mechanical design of hand, and mechanical design of forearm.

3.1. Requirements

By definition, an anthropomorphic hand must be anthropomorphic. While this does include someone unimportant details such as aesthetics, it also presents considerable limitations on size, which create formidable design constraints. In order to be considered sufficiently anthropomorphic, the apparatus will have to be approximately the same size and weight as its human counterpart. This means that not only the robotic hand must be the same size as a human hand, but that all of the actuators fit inside an apparatus approximately the same size as the human forearm.

The robotic hand itself must be capable of performing the same tasks that the hand is capable of performing. This requirement is both vague and difficult to accomplish. The concept of mechanical potential dexterity was introduced above. This concept will be applied to this

requirement:

From a purely mechanical standpoint (response time, forces, torques, workspace, etc.) the hand must perform to the same level of proficiency as the human hand. The design of the hand must include sufficient space for the addition of sensors, such that the mechanics of the hand do not interfere with the performance of the hand. The actuators of the hand must be adequately controllable such that a proficient control scheme could actually be implemented to control the hand dexterously.

3.2. Shape Memory Alloy

The decision to use thermal shape memory alloys for actuation creates a whole new set of decisions to be made. The most obvious is the selection of the specific shape memory alloy. Other parameters need to be determined such as cross-sectional area and length; these parameters are essential as they determine the performance of the apparatus.

There exist a wide variety of thermal shape memory alloys; those which are Nickel-Titanium alloys have significantly larger greater strains, stresses and work densities. The original alloy, Nitinol, is still commercially available. However, other similar alloys exist which are significantly cheaper that have the same performance; the performance characteristics among these alloys are all very similar. One specific alloy, Flexinol® is designed to be used in high-cycle applications. It was thus determined that since the robot hand would be undergoing many cycles, this alloy was the best choice.

The company that distributes Flexinol® offers two different standard alloys. The difference between these alloys is the associated transition temperature. One has a transition temperature of 70°C, and the other a transition temperature of 90°C; they also offer the option of a custom-made alloy at a requested transition temperature. An increased transition temperature

corresponds to a decreased cooling time, but it also corresponds to a higher required input energy, which means both lower efficiency and slower heating time for a given power input.

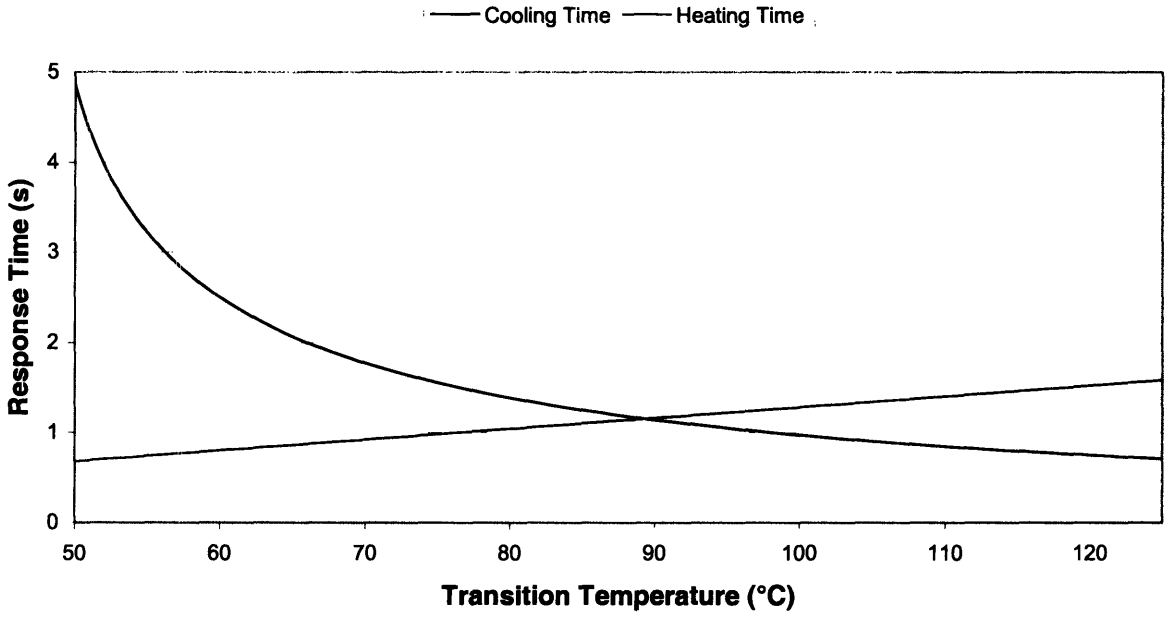

Figure 3: A comparison of the effects of increasing transition temperature on heating time and cooling time.

As can be seen from the above graph, the heating time of the shape memory alloy is linearly proportional to the

Selection of the diameter is a tradeoff between several parameters. The force delivered by the SMA is directly proportional to the cross-sectional area as seen by the equation

$$F = \sigma A_c \tag{18}$$

where F is the force, σ is the stress, and A_c is the cross-sectional area. Equations (12) and (14) show that the heating time is directly proportional to the cross-sectional area squared (assuming constant current) and that the cooling time is directly proportional to the diameter. Thus by increasing the diameter, forces are increased (improved) but response times are also increased (worsened).

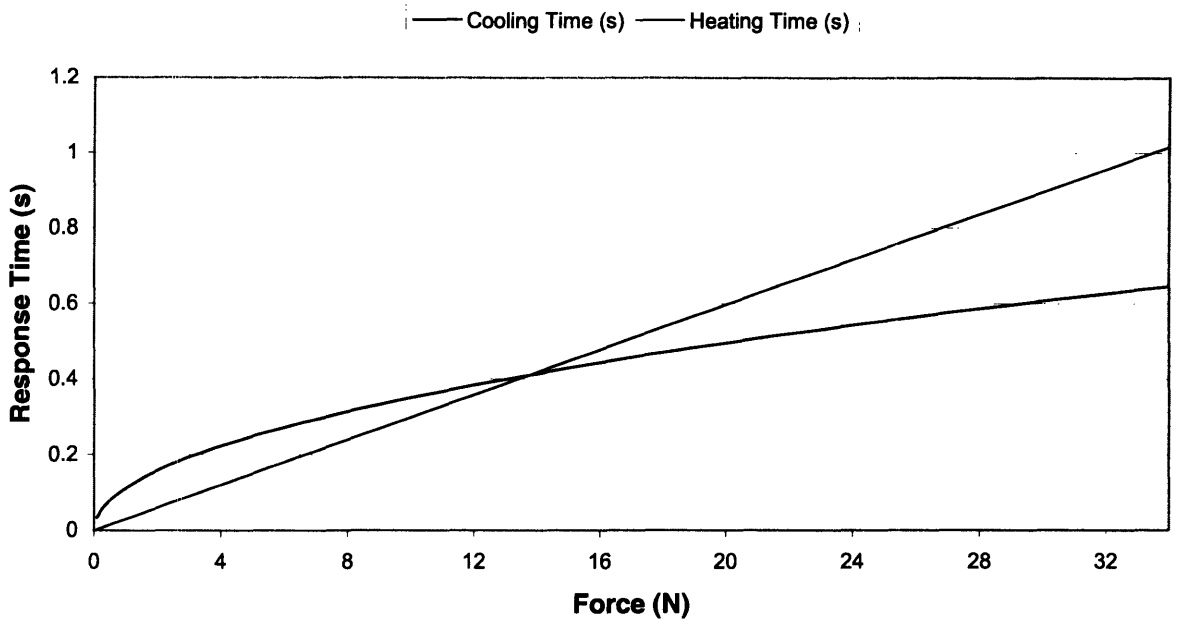

Figure 4: A plot of the response time of the actuator from (12) vs. the force delivered by the actuator from (15). These calculations were done by varying the input diameter while holding all other parameters constant. The heating time was calculated assuming adiabatic conditions and a constant input power.

As can be seen in Figure 3, the cooling time is linearly proportional to the diameter while the heating time is proportional to the cross-sectional area. These calculations are done for individual wires. The force delivered can be also be increased by adding multiple wires instead of individual ones. However, this increasing of the number of wires greatly increases the complexity of the system; the theoretical improvement in performance is outweighed by the actual decrease in performance due to complications.

The length of the wire was determined by design constraints within the hand, and will therefore be discussed in greater detail in section 3.4. The small strains made it such that the wires had to be relatively long. The length of the actuator was determined to be 12 inches.

3.3. Design Considerations of Cooling Mechanisms

Generally speaking, the limiting factor in response time is not the heating time; this can be improved by increasing the input power. The cooling time, however, is governed by the laws of thermodynamics. After the parameters of the actuator chosen, there are only two ways to improve the cooling time: The coefficient of convection can be increased, or the ambient temperature can be decreased. The effects of changing these parameters can be compared using equation (17). The cooling time as a function of ambient temperature can be seen below in Figure 5. The calculations for this graph were made holding all parameters except ambient temperature constant.

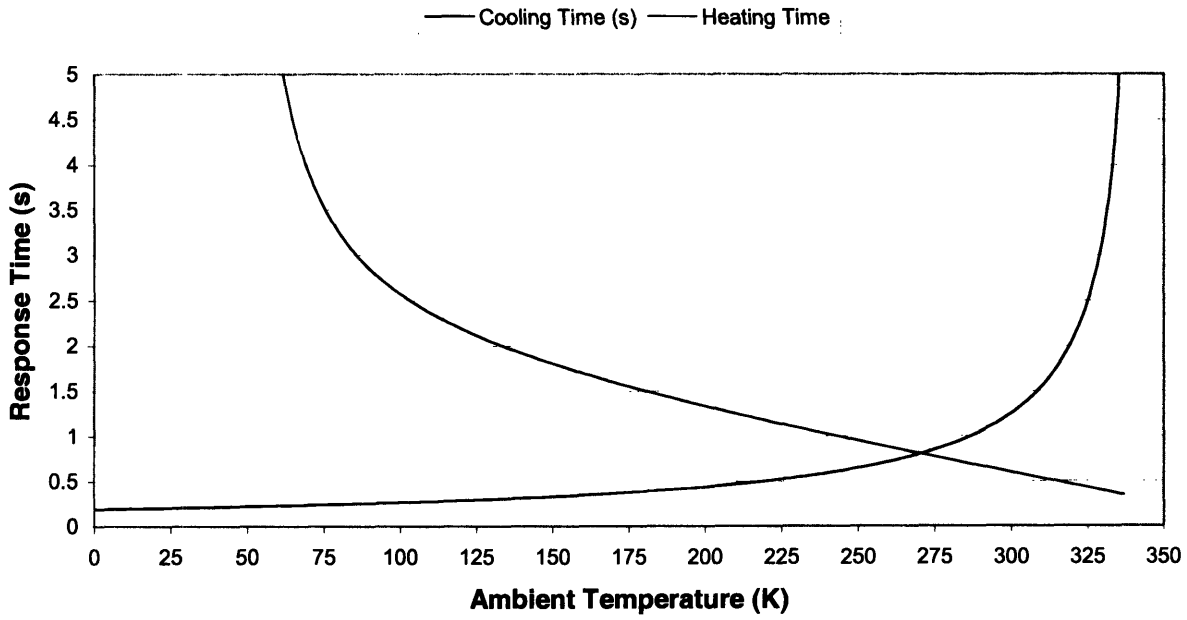

Figure 5: Heating and cooling time as a function of ambient temperature

As can be seen from the graph, decreasing the ambient temperature has positive effects on cooling time. However it has negative effects on the heating time as well. Modifying the ambient temperature, however, is not a practical task. It would involve either some form of refrigeration process, or the usage of some form of thermoelectric devices. The other option for

cooling is to improve convection. This can be done by changing the fluid in which the shape memory alloy is immersed. The other option would be to increase the velocity of the fluid. Once again, improving the cooling time has negative effects on the heating time, but as can be noted in Figure 6, these effects are much less extreme. Also to note, it is significantly less impractical to implement this improvement.

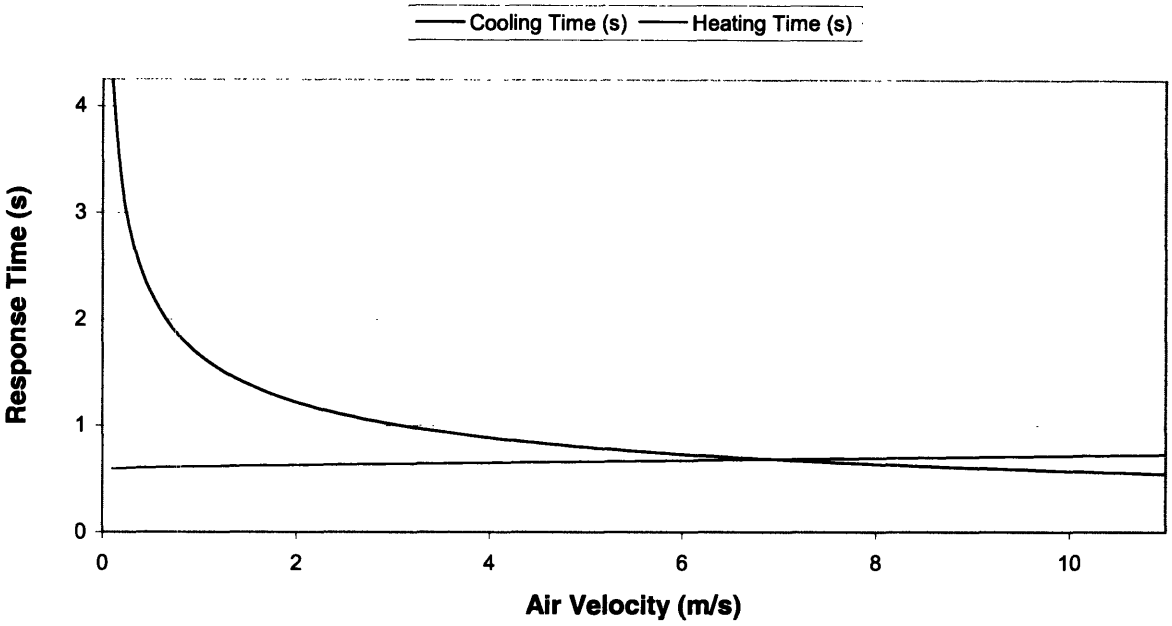

Figure 6: Response time as a function of air velocity.

Although it seems that the heating time is linearly dependent on the air velocity, the equation shows that it is not. The specific parameters of this application make it such that the detrimental effects of increasing the air velocity on the heating time are almost unnoticeable compared to the positive effects on the cooling time. The positive effects on the cooling time, however, seem to trail off after a certain velocity is attained. The velocity used by the fans in the robotic hand turn out to be 2.3 m/s; the limiting factor was the capabilities of the compact fans. A higher velocity fan would be advantageous.

3.4. Mechanical Design of Hand

The design of the hand was made with possibly the loosest and most abstract design constraints of the entire project. The hand was to be approximately the same size and shape of the human hand. It was to have a very similar workspace as the human hand and to be capable of sustaining similar forces and torques as the human hand. It was to be designed to include sufficient space for the placement of sensors.

Since no constraints were placed on the specifics of the design, it was decided that the simplest solution for every problem would be used. In most cases, this allows for a more reliable, robust design. The human hand has four fingers and a thumb; each finger has three joints and four degrees of freedom. Three of them are coplanar; the fourth is perpendicular to the plane made by the other three. It was decided that in order to have the same workspace as the human hand it would be necessary to include all degrees of freedom possessed by the fingers.

The fingers were designed in order to mimic the behavior of human fingers. In the human hand, while each finger possesses four degrees of freedom, only three are controlled. This makes it so that the human hand is underactuated. This underactuation allows the fingers to automatically conform to the shape of the surface of the objects to be manipulated without the intervention of controls. Underactuation is a simplistic and elegant method for grasping and thus will be included in the design.

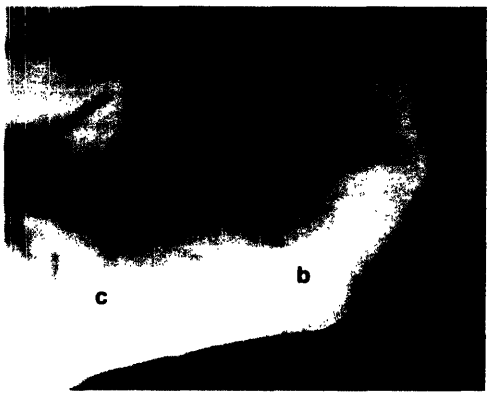

Figure 7: A human finger, bending at the joints

As can be seen in Figure 7, the human finger has three bones and three joints. The three bones at the base, middle and fingertip are known as the Proximal, Middle and Distal Phalanxes respectively. The joint labeled 'a' is known as the Distal

Interphalangeal Joint (DIP). The joint labeled as 'b' is known as the Proximal Interphalangeal Joint (PIP). The joint labeled as 'c' is known as the Metacarpal Phalangeal Joint (MCP). The coplanar motion that is achieved by these three joints is known as flexion and extension. The lateral motion done by the MCP joint is known as adduction and abduction. The motion achieved by the MCP joint is fully actuated. However, the motion of the PIP and DIP joints are coupled, and the control is shared.

The finger is actuated by muscles which are located in the forearm. The power from the muscles is transmitted to the fingers via tendons. One set of tendons for flexion and extension terminate in the Distal Phalanx; none terminate in the Middle Phalanx. This is why the motion is coupled and underactuated. The other tendons for flexion and extension as well as the tendons for adduction and abduction all terminate in the Proximal Phalanx. The motion of the thumb, however, is much more complex.

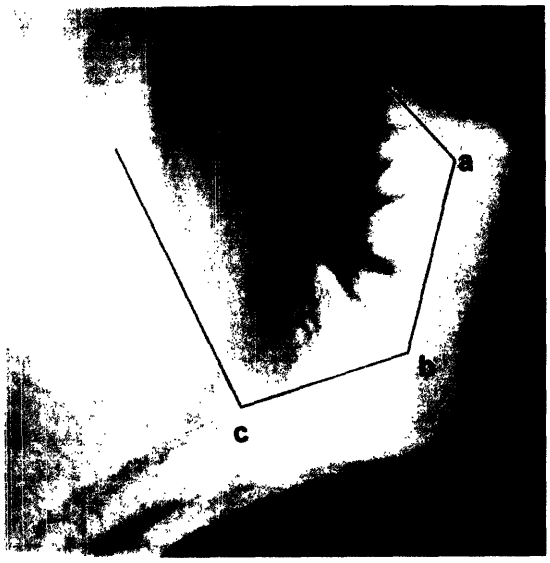

Figure 8: A human thumb

The human thumb consists of three bones, the Distal Phalanx, Proximal Phalanx and the First Metacarpal. The joints labeled 'a', 'b' and 'c' are the DIP, MCP and the Carpometacarpal (CMC) Joints respectively. Unlike the fingers, the motion of the thumb is fully actuated. The motion of the thumb is quite complex because the thumb is attached to the hand by a saddle joint. Approximating the motion for this type of joint is quite difficult. The joints labeled 'a' and 'b' undergo motion quite similar to their counterparts in the regular finger. The motion achieved by

the CMC joint can be divided into two distinct motions. One of the motions is perpendicular to the plane of joints 'a' and 'b'; this motion is analogous to the adduction/abduction motion of the MCP joint in the finger. The other causes the thumb to swing out in front of the palm. It is this motion which is responsible for the thumbs 'opposing' position in grasps.

The majority of the joints in human fingers are classified as hinge joints. Those that are not can be functionally reconstructed as hinge joints. In the design of the robotic hand, flexure joints were considered but dismissed. It has been claimed that flexure joints are the simplest solution. However, while they do consist of fewer parts, the complications that arise in application seem to indicate that flexure joints are not the simplest solution. Pin joints, on the other hand, very precisely replicate the motion of the human hinge joint. They are very simple, and are even capable of underactuation, in a similar fashion to the human hand, which is accomplished by tendon routing.

The tendons in the human hand themselves are very effective. One of the reasons is because the coefficient of friction is very low; the body produces a sort of natural lubricant. These tendons are routed in such a way as to allow the coupling of motion. The coupling of the motion can be seen quite clearly when the wrist is fully bent. Full extension of the fingers is difficult when the wrist is bent fully back; similarly full flexion of the fingers is difficult when the wrist is bent fully forward.

This coupling of motion significantly complicates controls. While it can be seen that the human hand is still fully functional, even with this coupling, it would be advantageous to minimize or eliminate this coupling as much as possible. This is not to say that the coupling should be removed altogether; certain types of coupling simplify controls, as indicated earlier.

It was decided to design the hand using a modular approach. Each of the four fingers

and the thumb would be designed to be completely removable from a central piece. This central part, of the size and the shape of the palm, would be how the hand is mounted to the forearm. Each individual finger would have four degrees of freedom. There would four individual segments and three coplanar pin joints. The final pin joint, which anchors the finger to the palm, would create motion perpendicular to the other joints.

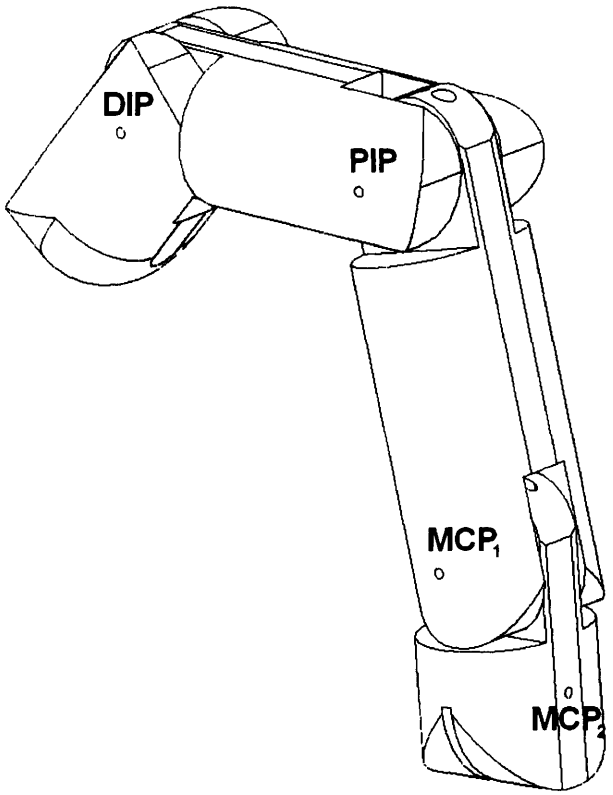

Figure 9: Robotic Finger

Since the only significant mechanical difference between any of the four fingers is the length, it was decided that all of the fingers on the robot would have the same mechanical design, such as tendon routing, joint configurations, diameter, but different lengths. This would turn out to be quite advantageous when applying controls because all of the fingers would possess the same kinematics. The fingers were the first part of the hand to be designed. Only after the design was tested and redesigned was a viable design of the thumb developed. This was because there were many issues with coupling and losses due to friction. The final design of the thumb mimicked the design of the fingers to a great extent. This should not be surprising since the anatomy of the thumb is very similar to the anatomy of the fingers.

The thumb was also designed to have four degrees of freedom. Its design was analogous to a finger with the PIP joint removed, but with an extra degree of freedom which allowed it to

swing out in front of the hand. It is to be noted that the thumb does not directly oppose the fingers in grasping motions. It actually is perpendicular. Intuitively, when people think of the pinching motion, they think that the thumb is perfectly opposite to the finger. The thumb was originally designed to accomplish this configuration, however it was found very quickly that in order to replicate the motion of the thumb without introducing extra degrees of freedom, a similar joint configuration is necessary.

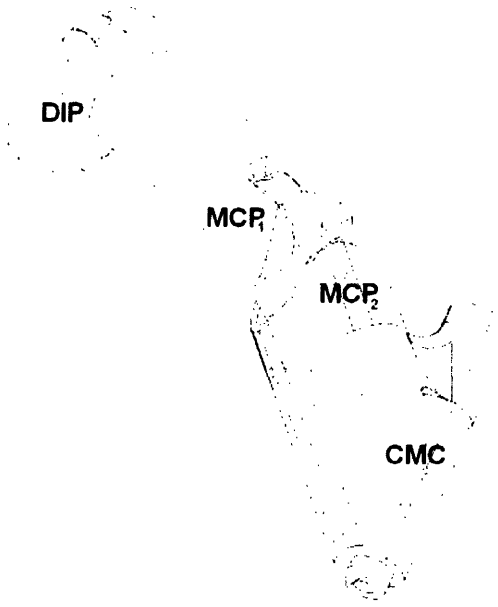

Figure 10: Robotic Thumb

The robotic thumb had four segments and four joints. It should be noted that some of the labels of the joints of the thumb in Figure 10 are the same as the labels of the joints of the fingers in Figure 9. The corresponding joints are almost identical. The only difference is the MCP_2 joint of the thumb has a larger range of motion. The CMC joint of the thumb, however, has no analogous joint in the finger. This too replicates the human hand. In both Figure 9 and Figure 10, small holes can be seen which do not correspond to pin joints. These holes locate tendon routing pins. These pins are included because the coefficient of friction of steel on Kevlar is significantly less than that of unfinished plastic on Kevlar.

These pins made for a significantly simpler internal structure of the plastic. Lateral holes replaced pulley-like structures, and voids replaced unnecessary long sheaths. Figure 9 shows an orthogonal view of the tendon routing within the finger. Since shape memory alloys are

unilateral actuators, the tendons were routed antagonistically to maintain full control, thus for controlled degree of freedom, there are two tendons. In the figure, the circles labeled 'P' correspond to the pins in the pin joints. The circles labeled 'RP' correspond to the redirecting pins, and the markers labeled 'T' correspond to points of tendon termination. As can be noted, no tendons terminate in the "Middle Phalanx" or the second most extreme finger; as such, the PIP joint is not independently controlled. The tendon which terminates at the fingertip, however, is routed in such a way that its length is affected by the DIP, PIP and MCP_1 joints. This coupling allows for the entire finger to be actuated by a single axis. However, the termination of the tendons in the Proximal Phalanx allow for complete control of the MCP_1 joint. This makes it such that the controller can choose the level of underactuation. The final set of tendons terminates in the base piece. This piece has no analogous bone in the human hand. The three coplanar joints, the DIP, PIP and MCP_1, can all undergo a motion of 90°. The third joint, the MCP_2, can bend 20° in either direction from its neutral position in the fingers; in the thumb, it can bend a full 45° from its neutral position.

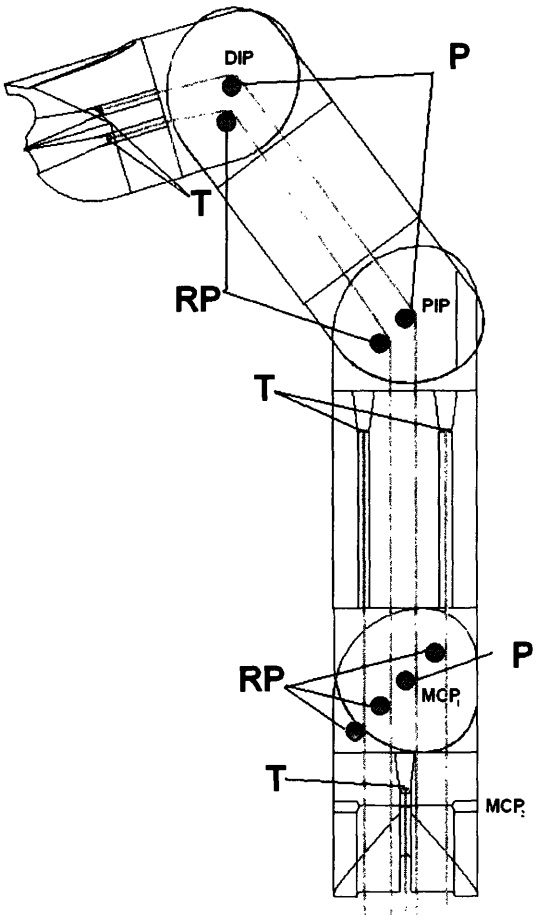

Figure 11: Orthogonal view of tendon routing.

Both sets of the flexion/extension tendons are routed through the center of the finger. This is so that there is no coupling associated with the movement of the MCP_2 joint. However,

since these are pin joints, the tendons are located in the exact same space as the pin would be. In order to be able to allow both of them to coexist, the pin for the pin joint is separated into two pieces. As can be seen in Figure 12, all of the tendons occupy a void, which is represented as the white space at the center. The black regions labeled MCP_2 correspond to the pins of the MCP_2 joint. It should be noted that these pins do not interfere with the cables, which are routed through the void. Figure 11 shows the tendon routing through the MCP segment; the three different angles of each tendon corresponds to the tendon configuration in its neutral position and at its travel limits in both directions. The MCP segment is the only piece that uses its own geometry as a pulley for the tendons. As stated earlier, the rest of the joints rely on metal posts. This is the only part of the entire hand that contacts the tendons in way other than as an anchor.

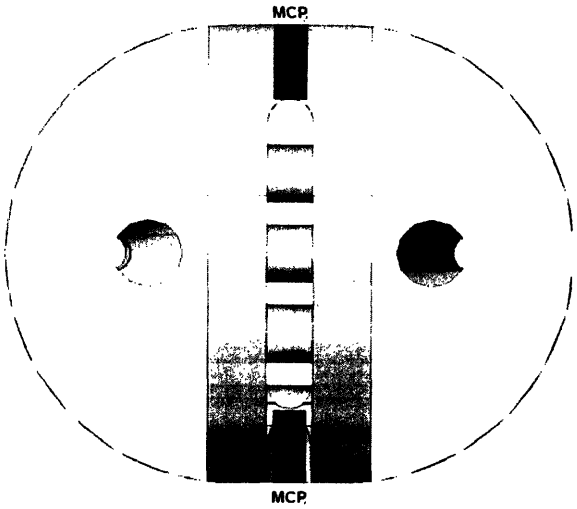

Figure 12: Front side view of MCP segment

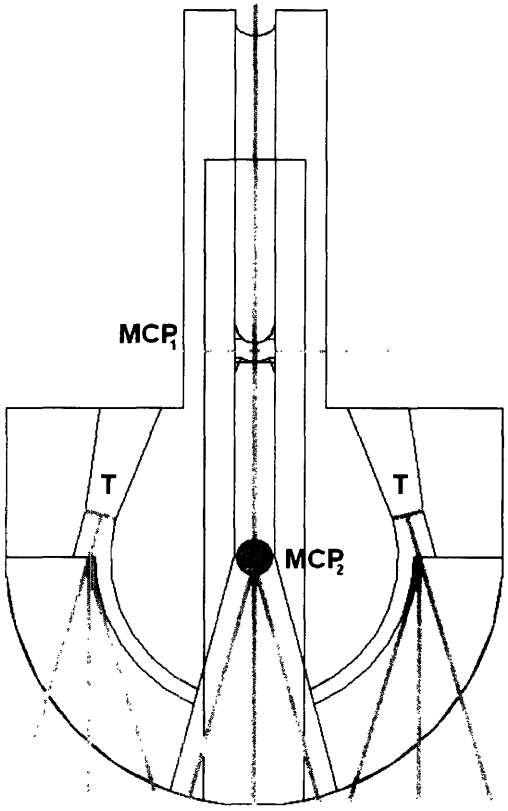

Figure 13: Tendon routing of MCP segment

As stated earlier, the first three segments of the thumb are exactly the same as three corresponding segments of the finger, but the base segment is completely different. This

segment is significantly larger than the other segments and undergoes a significantly greater displacement when moving. As such, without careful design, the coupling from the movement of this joint becomes severely detrimental to the performance of the thumb. It is this movement that makes the thumb opposable; it is arguably the most important feature of the thumb. Since it is the most difficult motion to replicate, it was tempting to just discard this motion; obviously, both the functionality and the anthropomorphicity would be detrimentally affected.

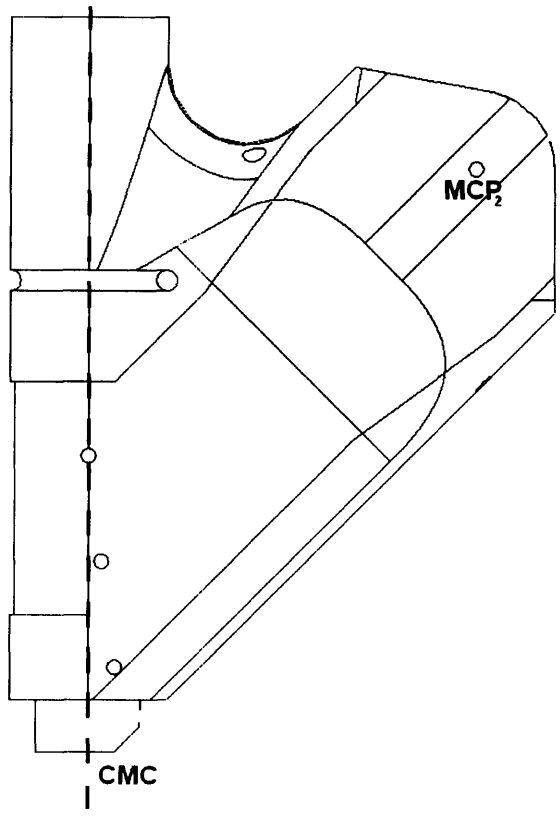

Figure 14: The thumb-base

The design of the thumb led to a minimal coupling due to this motion. However, the coupling was still severe enough to affect the performance. The coupling only affects the performance when the joint moves away from a specific position, a neutral position. Since the thumb is always opposing the hand when performing tasks, it was determined that this would be the natural position. When the thumb is pulled back, it has limited functionality; once again, this perfectly mimics the human hand. Motion is significantly more difficult for a human when the thumb is pulled back. The shaded region in the thumb represents a void in the material. The holes near the base are for steel posts which redirect the tendons from the rest of the thumb. The tendons exit the segment at the base.

The palm was designed so that the angles of the neutral positions of each of the fingers

caused the tendons to coalesce. Since the hand is wider than the wrist, it is necessary to move the tendons closer together before they enter the wrist region. This was accomplished, once again, by redirecting the tendons over steel posts.

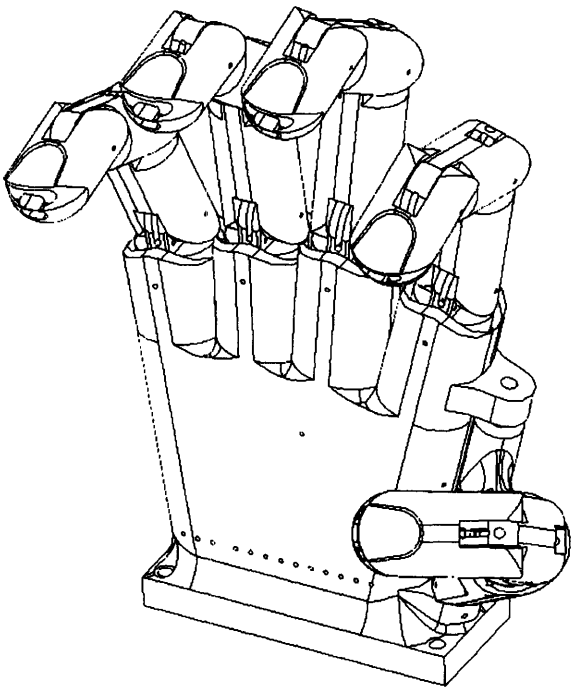

Figure 15: The entire hand

The CMC joint was designed to be different than every other joint in the hand. Every other joint had a steel post as the pin. This joint is formed by an extrusion at the base of the thumb fitting inside a hole in the base of the palm. This joint permits the tendons in the thumb to exit the palm and enter the wrist at the axis of rotation of the base of the thumb, allowing for a minimal amount of coupling with respect to the rotation of the thumb. Since there are 32 tendons running through an open space, it would seem that tangling would be a major issue. However, this is resolved in two ways. The first is by including an opening at the back of the hand. The tendons are each inserted one at a time, making sure that they are not tangled as they are introduced. The second is by keeping all of the tendons under tension at all times. The routing is such that the tendons do not cross paths. This helps minimize losses due to friction. A snap fit cover was

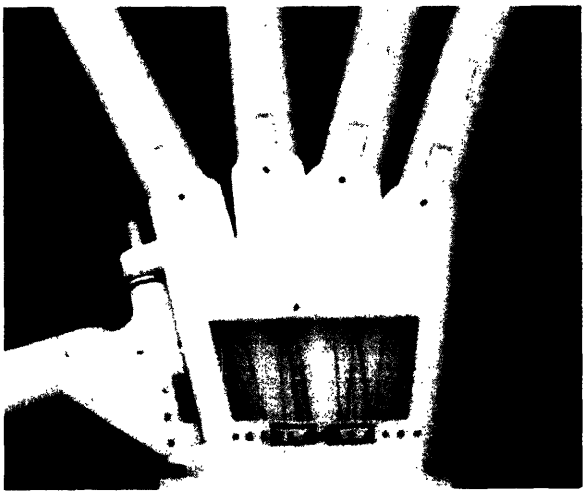

Figure 16: Tendon Routing

also designed to protect the cables from the introduction of outside debris.

3.5. Mechanical Design of Forearm

Due to the relative complexity of the system (despite the concerted efforts to simplify) the forearm was designed to allow for ease of assembly. The forearm was designed with an aluminum frame for support and a complex acrylic structure to hold the electronics and fans. Each was designed to be self-standing and independent.

The primary function of the aluminum frame was to sustain the substantial forces generated by the shape memory alloy actuators. The hand was thus anchored to one end of the aluminum frame; the SMA actuators terminated in the other side. Since the tension of the actuators was essential for proper performance, the actuators were threaded through the center of vented screws which were attached to the frame. As such, it was possible to adjust the length of the actuators and therefore control the tension.

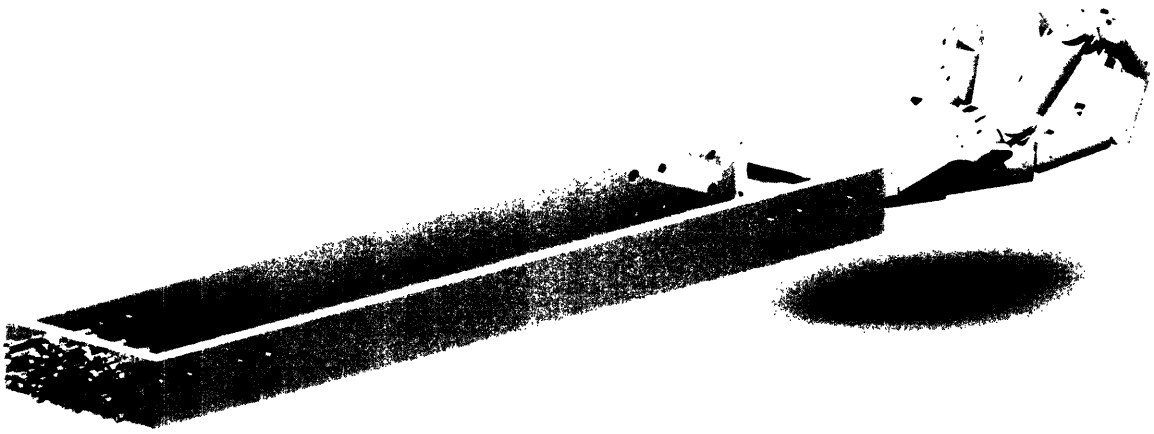

Figure 17: The Aluminum Frame

The structure was designed such that the SMA actuators were to be inserted and tightened before the addition of the acrylic substructure. This allows for a maximum amount of space for the assembler to connect the tendons to the SMA actuators. After all of the SMA actuators are

connected to the hand, the acrylic substructure can be added one piece at a time.

The acrylic substructure was designed with two main purposes. It served as an interface for the controller to actuate the SMA, and it served as a mounting point for the cooling fans. It consisted of three levels, the two upper levels served to anchor the electrical contact pins, the bottom level was designed to serve as a mounting point for the fans. Each SMA actuator was divided into 8 segments for controls. The segmentation was achieved by contact with steel posts which are spaced evenly throughout the length of the wires. The pins were designed to protrude a small distance from the surface of the acrylic cover. This flat surface with protruding metal pins makes for a very easy interface with a standard circuit board. As can be seen in Figure 18, the three levels are held in place by acrylic supports. The entire assembly was designed to be press-fit.

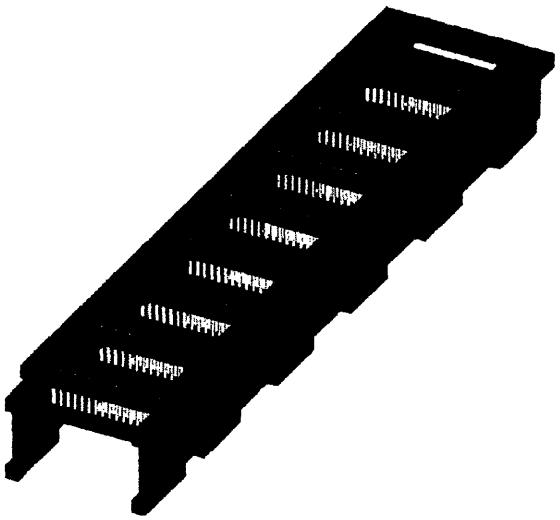

Figure 18: The Acrylic Structure

Figure 19: Assembly Process

In figure 19, a series of springs can be seen attached to the actuators. These springs serve to ensure that electrical contact is made in the desired fashion – to the contact posts and not to the other wires. These springs are designed with a travel limit; as such they do not interfere with

controls.

In assembly, after all of the SMA actuators are installed under tension in the aluminum frame, the next step is to remove one side of the frame. An acrylic support can be slid past the actuators and anchored to the aluminum frame. The middle level acrylic plate can then slid in between the two antagonistic levels of actuators (flexion and extension). The aluminum plate which was removed can now be replaced after being anchored to the other acrylic support. The top and bottom layers of acrylic can then be attached to the assembly, and the fans can then be anchored to the base. The final step in the mechanical assembly is to insert the electrical contact pins. Once the pins are in place, the hand is ready to be fitted with circuit boards and controlled.

4. Performance Evaluation

This section summarizes the performance of the robotic hand. However, as stated in section 1.2, the specific kinematic parameters do not in any way reflect the dexterity of the hand. The efficacy of the hand must be measured on a much more functionalistic scale. Unfortunately, a controller has yet to be implemented, and as such, any remarks on actual performance are purely conjecture.

4.1. General Performance

In its final state, the robot arm weighs just over 3 lbs; not including the fans, the forearm is 1.5"x3"x15". This is approximately the size of a human forearm. As to the actual performance of the robotic hand, everything that was built as designed performs as designed. There were some slight complications which arose from deviations from design.

The only deviation from the original design was the usage of screws with radially drilled holes rather than axially. This was because the cost of the vented screws (with holes down the axis) is actually more than the rest of the materials for the entire assembly! This says two things:

the cost of the vented screws is quite high (~$4 each), and that the cost of the rest of the materials for the robotic hand is very low (~$100).

However, it turns out that the vented screws are necessary in order to yield the desired performance. When the radially drilled screws were turned to achieve the desired level of tension, the actuators would act as torsional springs, loading themselves as the screw was twisted. While the static friction was sufficient to hold the screws in place initially, as soon as the material underwent its phase transition, the screws would spin and the wire would slack as soon as the actuator would relax. Once the more expensive screws were implemented, the performance became as predicted.

4.2. Kinematics

The geometry of the internal structure of the hand allows for very simple kinematics of the extensor tendons, but very complex kinematics for the flexor tendons. Almost all of the joints have the same configuration, (all but the MCP_2 joints) so the calculations only have to be done once.

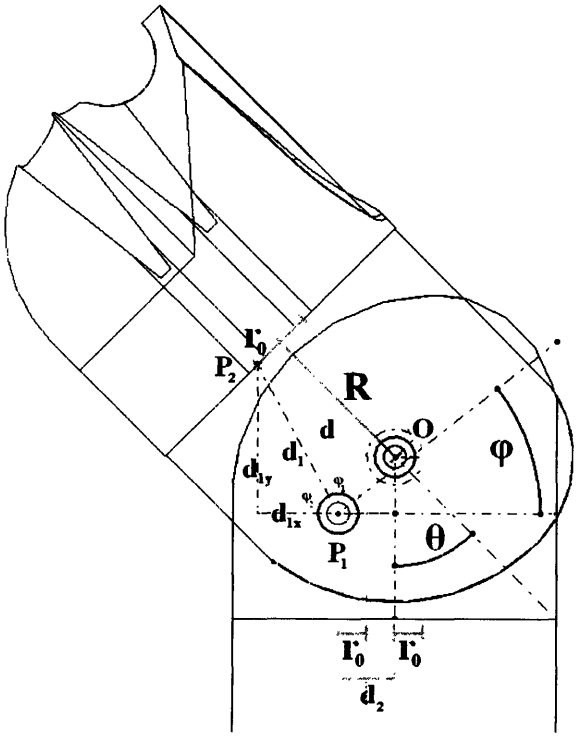

Figure 20: Kinematics of finger

The change in length of the extensor due to a change in angle, θ, is simply given by the equation

$$\Delta l = (R + r_0\theta) - (R) = r_0\theta \qquad (19)$$

where l is the length of the tendon, and R and r_0 are known dimensions of the finger. Very similarly, the equation for the flexor is

$$\Delta l = (d + r_0\phi) - (R) \qquad (20)$$

where R and r_0 are once again known dimensions of the finger. However, d and φ are configuration dependent. The length of d can be calculated from the equation

$$d = \sqrt{d_1^{\,2} - r_0^{\,2}} \tag{21}$$

where d_1 also needs to be calculated. The length of d_1 can be found by calculating the distance from P_1 to P_2.

$$\vec{d}_1 = \vec{P}_2 - \vec{P}_1 \tag{22}$$

The position of P_1 (distance from O) is described by the following equation:

$$\vec{P}_1 = \begin{bmatrix} -d_2 \\ -d_2 \end{bmatrix} \tag{23}$$

it can be noted that since P_1 is fixed, it does not change when θ is changed. The position of P_2, however, does change with θ, and as such is significantly more complex:

$$\vec{P}_2 = \begin{bmatrix} -r_0 \cos\theta - R\sin\theta \\ -r_0 \sin\theta + R\cos\theta \end{bmatrix} \tag{24}$$

Equations (21)-(24) fully describe d in terms of known parameters. However, in order to solve (20), φ too must be calculated. φ is described by the equation

$$\phi = \pi - (\phi_1 + \phi_2) \tag{25}$$

where φ_1 and φ_2 are expressed in radians. φ_1 is described by the equation

$$\cos\phi_1 = \frac{r_0}{d_1} \tag{26}$$

and φ_2 is described by the equation

$$\tan\phi_2 = \frac{d_{1y}}{d_{1x}} \tag{27}$$

combining equations (20)-(27) we arrive at an expression for the flexion motion:

$$\Delta l = \begin{pmatrix} \sqrt{(d_2 - r_0\cos\theta - R\sin\theta)^2 + (d_2 - r_0\sin\theta + R\cos\theta)^2 - r_0^2} \\ + r_0\pi - \arccos\left(\dfrac{r_0}{\sqrt{(d_2 - r_0\cos\theta - R\sin\theta)^2 + (d_2 - r_0\sin\theta + R\cos\theta)^2}}\right) \\ - \arctan\left(\dfrac{d_2 - r_0\sin\theta + R\cos\theta}{d_2 - r_0\cos\theta - R\sin\theta}\right) - (R) \end{pmatrix} \tag{28}$$

This equation is rather large and cumbersome. Finding the inverse kinematics for this would be quite difficult. However, Figure 21 shows that the parameters of the finger make it such that the equation can be approximated quite effectively as linear.

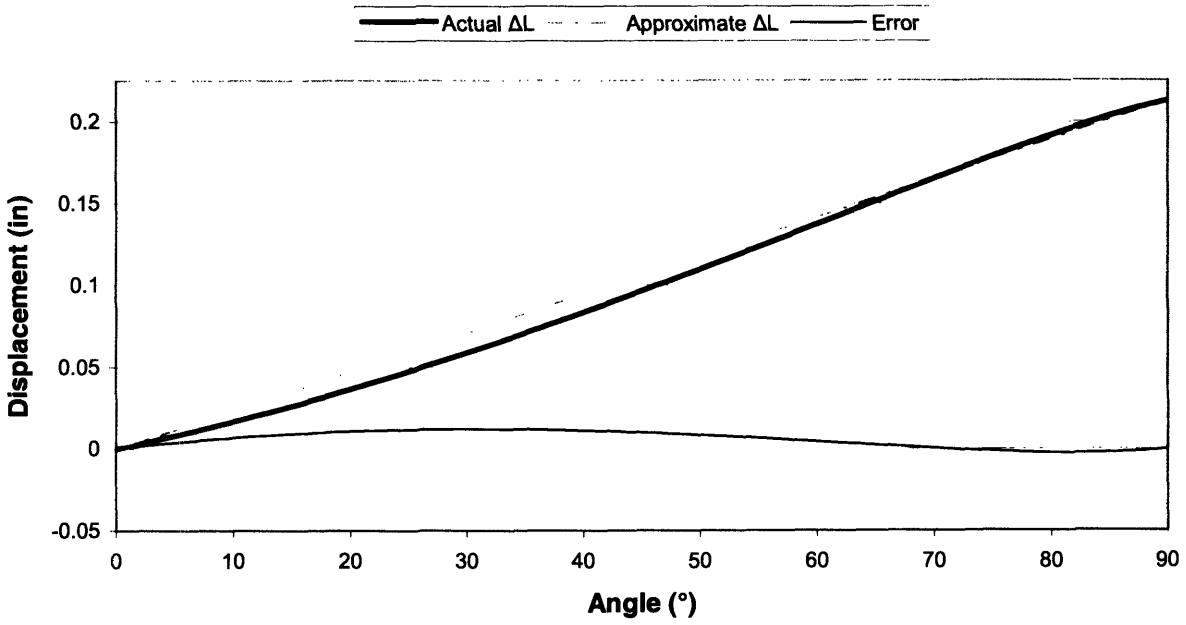

Figure 21: Tendon displacement as a function of angular displacement

A linear approximation works sufficiently for a relation between angular displacement and tendon displacement. In order to find the Jacobian, the differential must be calculated. The error from using the above approximation would be severely increased by differentiation. In order to get a more precise number, either the actual differential must be calculated, or a more precise approximation must be made. However, the losses due to friction in the joints make it

such that a precise calculation would not yield useful information. Using the linear approximation, the expected torques delivered by the hand are around 67 N·mm. Crude testing yielded values closer to 40 N·mm, but this is to be expected.

The response times calculated for the heating and cooling time were 0.627 s and 1.14 s respectively. Testing showed that the heating time was closer to 0.3 s and the cooling time to 1.5 s. Although the heating time was off by a factor of 2, this is to be expected because the little information that is available on the material is not highly accurate. The material does not all undergo the phase transition at the specified transition temperature; this is one reason that the experimental data deviated from the theoretical model. Similarly, the correlation for the cooling time is known to only be around 10% accurate.

Not much testing was done on the specific parameters (reaction time, forces etc.) because the main interest is simple functionality. The torques produced by the fingers are definitely sufficient to manipulate objects for general grasping purposes. The fingers react somewhat slowly to moderate amperages (~2-3) and much more quickly to larger amperages (~4-6).

4.3. Workspace

The workspace of the mechanical hand was designed to recreate that of the human hand. The approach was to mimic the behavior of each of the individual joints, arranging them in an identical configuration. The PIP, DIP and MCP_1 joints were designed to have a 90° range of motion; the MCP_2 joint was designed to have a 40° range of motion.

In the actual model, the PIP and DIP joints do have the full designed range of motion. However, the MCP joints have a slightly reduced range of motion. In the MCP_1 the mechanical constraints of the palm which provide the torsional support impede the movement; the actual range of motion for this joint is closer to 85°. The tendons in the MCP_2 joint can only move it

15° from the neutral position in either direction; the finger, however, is still capable of undergoing a 20° displacement before the joint reaches the mechanical stop.

The current hand is made almost entirely out of ABS, and as such is very incompliant and low coefficient of friction. However, even with frictionless contacts, the robotic hand is still capable of fully constraining objects up to 2.75 inches in diameter. The hand is also capable of constraining objects of very small diameter as well. This is accomplished by the concave "fingernail" spaces in the upper half of the fingertips. The fingers were able to be arranged in such a way as to hold even a paper clip. By causing the hand to cycle through its travel limits, it was shown that the robotic hand has approximately the same range of motion as the human hand.

5. Conclusion

Expressing the performance of robotic hands in words is a relatively difficult task. A list of the objects that the hand is capable of grasping can be given, numbers such as response time, finger torques and range of motion can be listed. However none of these capture the true performance of the hand. Generally, when a robotic hand is capable of a noteworthy task, a video is published showing the task performed. Many of the accomplishments of this project are not quantifiable. However, much progress was made in the field of robotic hands, as will be explained below.

5.1. Progress

By far, the largest stride in robotics from this project was the sheer simplicity of the project. With $200 worth of materials which weight a total of 3 lb, a 32 actuator box of dimensions 1.5"x3"x14" was manufactured which controls a 20 degree of freedom (16 controlled) robotic hand. The simplistic design allows for very reliable, repeatable results.

This improvement was made possible by the usage of thermal shape memory alloy

actuators. The implementation of these actuators was made practical by the introduction of two concepts: segmentation and travel-limited compliance. The idea of segmentation simultaneously simplifies and limits controls: a very complex nonlinear actuator with hysteresis can now be very simply controlled with very limited modeling. However, the resolution which the actuator can accomplish is hard-limited by the mechanical configuration.

The introduction of travel-limited compliance allows for the actuator to guarantee contact with the electrical apparatus. The introduction of compliance to the system under normal circumstances would create issues with controls. However, the limited travel makes it such that controls are not affected at all.

5.2. Further Work to be Done

A significant amount of work has yet to be done in order for the hand to perform as an efficient robotic hand. At the very least, sensors have to be added and a control scheme must be implemented in order for the hand to function at all. However, there exist many other mechanical improvements that could be implemented which would serve to improve performance even further. The distinction must be made, however, between the improvement of the current hand and advancements in the field of robotics.

It truly is necessary to implement a control scheme with sensors in order to ensure the efficacy of the materials as actuators for dexterous applications. However, mechanical adjustments, such as the introduction of compliant materials to improve grasp stability, would be solely an improvement in the robotic hand. A robotic hand which integrates all of the relevant research that has been done in the past 20 years, however, would indeed bring the field a step further. As such as many improvements as necessary will be implemented in the next iteration.

From the perspective of biomimetics, the greatest gap between current robotic systems

and human physiology is sensors. A human hand has thousands and thousands of sensors situated in arrays which sense contact, force and temperature. In order for a robotic hand to ever be able to recreate the functionality of the human hand, at the very least the capabilities of these arrays of sensors must be realized. The next step, after a simple control scheme is implemented, is to develop a sensor system which matches the performance of the analogous human system.

5.3. Final Remarks

A robotic hand was designed and built which is significantly smaller and lighter than any other before it. It promises to be a very effective robot hand, but claims of efficacy cannot be made until a proper control scheme is implemented. However, progress was definitely made in the field of compact actuators. Segmentation has proven itself the best possible method of actuation for shape memory alloys.

References

[1] Okada, T.: 1986, Computer Control of Multijointed Finger System for Precise Object Handling, *International Trends in Manufacturing Technology – Robot Grippers.*

[2] Salisbury, K. and B.Roth: 1983, Kinematics and force analysis of articulated mechanical hands, Journal of Mechanisms, Transmissions and Actuation in Design, 105.

[3] Jacobsen, S., Iversen, E., Knutti, D., Johnson, R. and Biggers, K.: 1986, Design of the Utah/MIT dexterous hand, Proc. IEEE International Conference on Robotics and Automation, ICRA86.

[4] Melchiorri, C. and Vassura, G.: 1992, Mechanical and control features of the UB hand version ii, Proc. IEEE/RSJ Int.Conf.on Intelligent Robots and Systems, IROS'92.

[5] Butterfass, J., Grebenstein, M., Liu, H. and Hirzinger, G.: 2001, DLR hand ii: Next Generation of a Dexterous Robot Hand, Proc. IEEE International Conference on Robotics and Automation, ICRA01, Seoul, Korea.

[6] L. Biagiotti, F. Lotti, C. Melchiorri, G. Vassura "How Far Is the Human Hand? A Review on Anthropomorphic Robotic End-effectors"

[7] Huxley, A.F. *Reflections on Muscle.* Princeton University Press: Princeton, New Jersey, 1980.

[8] I. Hunter and S. Lafontaine, "A Comparison of Muscle with Artificial Actuators," in *Tech. Dig. IEEE Solid State Sensors Actuators Workshop*, 1992, pp. 178–185.

[9] J. Madden, N. Vandesteeg, P. Anquetil, P. Madden, A. Takshi, R. Pytel, S. Lafontaine, P. Wieringa, and I. Hunter, "Artificial Muscle Technology: Physical Principles and Naval Prospects", IEEE Journal Of Oceanic Engineering, Vol. 29, No. 3, July 2004

[10] Purves, Sadava, Orians, Heller, "Life the Science of Biology" Sinauer Associates, Inc, 2004.

[11] K.J. Cho, J. Rosmarin, H.H. Asada, "Design of vast DOF artificial muscle actuators with a cellular array structure and its application to a five-fingered robotic hand," in Proceedings of the IEEE International Conference on Robotics and Automation, 2006.

[12] S.W. Churchill and M. Bernstein, A correlating equation for forced convection from gases and liquids to a circular cylinder in cross-flow. *J. Heat Transfer, Trans. ASME, Ser. C,* 99:300-306, 1977.

Appendix I: SMA Datasheet

NICKEL - TITANIUM ALLOY PHYSICAL PROPERTIES

1. Density	0.235 lb/in^3 6.45 g/cm^3
2. Specific Heat	0.20 BTU/lb.-°F 6-8 cal(mol °C)
3. Melting Point	2282 °F 1250 °C
4. Heat of Transformation	10.4 BTU/lb
5. Thermal Conductivity	10.4 BTU/hr-ft-°F 0.05 cal(cm-°C-sec)
6. Thermal Expansion Coefficient	
Martensite	3.67x10^{-6}/°F 6.6x10^{-6}/°C
Austenite	6.11x10^{-6}/°F 11.0x 10^{-6}/°C
7. Electrical Resistivity	
Martensite	421 Ohms/Cir Mil Ft (approx.)
Austenite	511 Ohms/Cir Mil Ft (approx.)
8. Linear Resistance (approx.)	
.003 inch diameter wire	4.3 ohms/inch
.005 inch diameter wire	1.7 ohms/inch
.006 inch diameter wire	1.25 ohms/inch
.010 inch diameter wire	0.44 ohms/inch

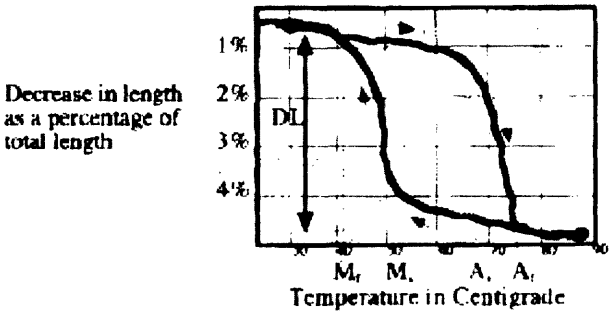

Figure 1. Change of length of Flexinol™ (70° C transition temperature) with change in temperature while constant tensile stress is applied to the wire.